Evolution of the reaction dynamics in the interaction of copper with 15–90 MeV/nucleon ^{12}C ions

J. P. Whitfield and N. T. Porile
Department of Chemistry, Purdue University, West Lafayette, Indiana 47907
(Received 3 September 1992)

Target residues from the interaction of copper with 90 MeV/nucleon ^{12}C ions have been studied using thick-target, thick-catcher recoil range techniques. Cross sections, average ranges, and forward-to-backward ratios have been measured. Isobaric and mass yield distributions, along with mean longitudinal momentum transfer and mean excitation energy, have been obtained from these data. Comparisons with previous 15–45 MeV/nucleon ^{12}C + Cu results and with intranuclear cascade and evaporation models are presented.

PACS number(s): 25.70.Mn

I. INTRODUCTION

As beam energies increase from the low-energy regime (<10 MeV/nucleon), mean-field dominance of the reaction mechanism, signified by complete fusion, gives way to increasing incomplete fusion and begins to show traits of high-energy reactions (>100 MeV/nucleon). It is in this high-energy regime where nucleon-nucleon interactions become increasingly important. An understanding of this evolution from mean-field to nucleon-nucleon dynamics has generated great interest in the past decade.

Two important characteristics of the reaction which help in understanding the evolution of the reaction dynamics are E^*, the excitation energy deposited in the composite system, and the linear momentum transferred (LMT) from the projectile to the target nucleus in the initial interaction. As accelerators have become able to deliver a wide variety of heavy-ion beams at various energies, some interesting phenomena have been reported. Galin *et al.* [1] found that the maximum LMT reached a constant value of approximately 2 GeV/c, independent of bombarding energy, for the interaction of ^{12}C + Au and U. Further studies utilizing various projectile-target combinations [2–6] revealed that LMT seemed to saturate at ~180–220 MeV/c per incident nucleon. This saturation was reached at approximately 25–35 MeV/nucleon independent of projectile or target identity. It was also noted [7] that there was a total disappearance of complete fusion by 35 MeV/nucleon. Other results [8, 9] have also suggested a limitation to the excitation energy which can be deposited in the residual nucleus, beyond which the nucleus becomes extremely unstable and may multifragment [10]. Many of these data have been obtained for fissionable targets using folding angle techniques.

Recently, lighter targets have been studied. Utilizing recoil-range techniques, Pieńkowski *et al.* [11] have reported on the interaction between Ne and Cu at 8–48 MeV/nucleon. Many other studies [12–17] have also reported on various target-projectile combinations using these techniques. Cho *et al.* [18, 19] have studied the interaction of copper with 15–45 MeV/nucleon ^{12}C ions by means of these techniques. In this work these measurements are extended to 90 MeV/nucleon in order to permit a study of the evolution of the reaction mechanism over a wider energy regime.

II. EXPERIMENTAL DETAILS

A 90 MeV/nucleon ^{12}C ion beam, ~10 enA in intensity, was employed using the K1200 cyclotron at the National Superconducting Cyclotron Laboratory (NSCL) at Michigan State University. The beam intensity was measured by means of a Faraday cup and recorded with a current integrator. The beam was incident on a 20.1 mg/cm^2 ^{nat}Cu target surrounded by forward and backward carbon catcher foils of 10.1 mg/cm^2 areal density. Guard foils, again of carbon (10.1 mg/cm^2), were also utilized to measure direct activation of the catcher foils. The energy of the beam at the center of the target stack was determined to be 1073 MeV, on the basis of energy loss in the carbon and copper foils [20]. A 30 min irradiation was performed in order to obtain information for the short-lived products. A second irradiation of longer duration, 6 h, was run for the longer-lived products. Following irradiation, the various foils were assayed utilizing calibrated Ge and Ge(Li) γ-ray spectrometers. For the short irradiation, foils were counted at NSCL for approximately 24 h. Assay began approximately 30 min after the end of bombardment (EOB). For the long irradiation the foils were returned to Purdue and counting began 1 day after EOB and continued for several months. γ-ray intensities were determined with the code SAMPO [21]. From these intensities decay curves were constructed and subsequently analyzed using the code CLSQ [22]. Nuclidic assignments were made on the basis of γ-ray energy, half-life, and association with other γ rays emitted from an inferred nucleus [23].

III. RESULTS

One of the most appealing features of thick-target, thick-catcher, off-line γ-ray techniques is the ability to

 ©1993 The American Physical Society

measure cross sections and average kinematic properties of individual radioactive nuclides. The production cross sections for the individual products are listed in Table I. Cross sections were obtained by summing the measured activity from the target and catcher foils. For those products for which more than one γ ray could be detected, from either the long or short irradiations, the values are weighted averages over the complete set of γ-ray energies. The uncertainty in these values corresponds to the larger of the standard deviation of the mean value and the estimated uncertainty in the individual values. These uncertainties have several contributing factors, e.g., error propagation from CLSQ and SAMPO fits, detector efficiencies, and beam intensity determination. Nuclides for which only one determination of a single γ ray was made had an additional uncertainty of 10% folded in. The ^{22}Na cross section was reduced by ~16% in order to correct for direct production in the carbon catcher foils. None of the other cross sections required an activation correction.

TABLE I. Cross sections, forward ranges, and forward/backward ratios for product nuclides from the interaction of copper with 90 MeV/nucleon ^{12}C ions.

Nuclide	Type	σ (mb)	FW (mg/cm^2)	F/B
^{22}Na	C^+	2.62±0.29	3.42±0.46	21.3±8.0
^{24}Na	C^-	4.71±0.52	2.96±0.37	22.3±5.5
^{28}Mg	C^-	0.48±0.03	2.75±0.19	
^{34}Cl^m	C^+	1.35±0.18	2.56±0.58	4.48±2.48
^{39}Cl	C^-	0.90±0.03	2.70±0.36	
^{41}Ar	C^-	1.55±0.18	1.75±0.26	
^{42}K	I	8.24±0.94	1.75±0.27	
^{43}K	C^-	2.50±0.08	1.51±0.11	41.5±2.9
^{43}Sc	C^+	9.30±1.14	1.17±0.18	
^{44}Sc	I	6.77±0.82	1.54±0.22	
^{44}Sc^m	I	15.6±1.5	1.49±0.14	118±17
^{46}Sc	I	16.0±0.2	1.37±0.02	198±21
^{47}Ca	C^-	0.15±0.02	1.95±0.72	
^{47}Sc	I	6.69±0.72	1.12±0.12	86.3±7.5
^{48}Sc	I	1.09±0.09	0.59±0.07	42.7±15.1
^{48}V	I	23.7±0.3	1.22±0.02	145±20
^{48}Cr	C^+	0.74±0.03	1.16±0.02	26.2±2.2
^{49}Cr	C^+	5.82±0.51	1.16±0.12	
^{51}Cr	C^+	65.0±6.9	0.97±0.11	82.9±15.3
^{52}Mn	I	14.2±0.8	0.93±0.05	115±14
^{52}Mn^m	I	3.95±0.56		
^{52}Fe	C^+	0.42±0.05	0.99±0.15	
^{54}Mn	I	49.7±5.2	0.80±0.09	61.0±4.6
^{55}Co	C^+	2.74±0.15	0.69±0.06	
^{56}Mn	C^-	6.33±0.05	0.73±0.02	
^{56}Co	I	16.9±0.5	0.62±0.03	
^{56}Ni	C^+	0.13±0.01		
^{57}Co	I	62.0±1.8	0.53±0.02	44.5±1.4
^{57}Ni	C^+	2.00±0.04	0.51±0.04	
^{58}Co	I	67.7±5.5	0.49±0.04	34.0±0.5
^{59}Fe	C^-	3.67±0.02	0.42±0.05	
^{60}Co	I	20.4±0.9	0.31±0.02	
^{60}Cu	C^+	8.20±0.17		
^{61}Cu	C^+	34.2±1.6	0.24±0.02	
^{62}Zn	C^+	8.32±0.14	0.25±0.05	
^{63}Zn	C^+	4.97±0.20		
^{64}Cu	I	51.8±8.0		
^{65}Ni	C^-	0.53±0.12		
^{65}Zn	C^+	3.84±0.42	0.37±0.09	

Most of the tabulated cross sections are actually cumulative yields, where products along a given β isobaric chain have contributed to the measured value. These are denoted by C^+ for products from proton-rich progenitors, while C^- denotes those with contributions from neutron-rich progenitors. Those where there is no progenitor contribution are labeled I, independent.

The results of the recoil measurements can be expressed in terms of the average forward range FW and the forward-to-backward ratio F/B, where W is the thickness of the target in mg/cm^2 and F and B are the fraction of total activity collected in the forward and backward catchers, respectively. Corrections to FW due to direct activation of the carbon catcher foils had to be applied to four products in addition to ^{22}Na. The corrections to the former were ~3%, while that to the latter was ~23%. The F/B values listed in Table I reflect corrections in both the forward and backward catchers due to direct activation of these foils.

Lund *et al.* [14] have previously reported the results of cross-section and recoil-range measurements for products of the interaction of copper with 86 MeV/nucleon ^{12}C. The two data sets are compared in Fig. 1, which shows the variation with product mass of the ratios of cross sections and FW values. The two data sets generally agree moderately well, although the present FW values tend to be smaller than the earlier ones. The difference is in line with the decrease in FW observed between 45 and 90 MeV/nucleon [19].

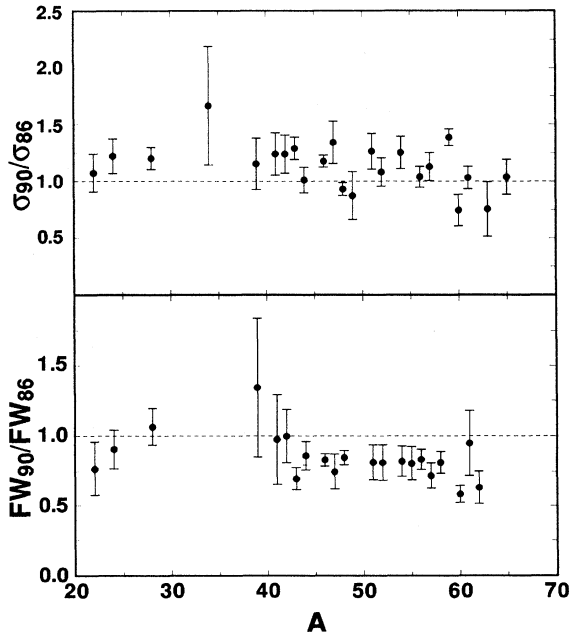

FIG. 1. Ratios of present cross sections (top) and FW (bottom) to the corresponding quantities reported for the interaction of copper with 86 MeV/nucleon ^{12}C [14].

TABLE II. Parameters utilized in the fit of Eqs. (1) and (2) to experimental cross sections from the interaction of copper with 90 MeV/nucleon ^{12}C ions.

Parameter	Value	Parameter	Value
α_1	2.52±0.70	α_6	−0.19±0.02
α_2	−0.26±0.05	α_7	(2.15±0.16) $\times 10^{-3}$
α_3	(1.11±0.12) $\times 10^{-2}$	α_8	1.52±0.03
α_4	−(1.06±0.10) $\times 10^{-4}$	α_9	0.48±0.00
α_5	2.22±0.37	α_{10}	−(2.82±0.10) $\times 10^{-4}$

IV. DISCUSSION

A. Isobaric yield distribution

Radioactive products represent only a fraction of the total reaction cross section. Therefore we must estimate the cross sections of products undetectable by our experimental methods, for example, very short-lived or stable products. Rudstam [24] proposed a six-parameter equation for spallation products, assuming that the mass yield curve decreases exponentially with decreasing mass number and the isobaric yield distribution is Gaussian at a given mass number. In our previous work [18, 19] this equation was unable to fit the complete product mass region, specifically the low-mass region, where there is an upturn in the mass yield distribution. Furthermore, the Rudstam equation was unable to fit the isobaric yield distribution. Therefore a ten-parameter modified version of the equation has been utilized [25]:

$$\sigma(Z,A) = \exp[\ \alpha_1 + \alpha_2 A + \alpha_3 A^2 + \alpha_4 A^3 + (\alpha_5 + \alpha_6 A + \alpha_7 A^2)|Z_p - Z|^{\alpha_8}], \quad (1)$$

where

$$Z_p = \alpha_9 A + \alpha_{10} A^2. \quad (2)$$

Equation (1) consists of terms determining the mass yield distribution (α_1–α_4) and the width of the isobaric distribution (α_5–α_7). The parameter α_8 determines the shape of the isobaric distribution, where $\alpha_8 = 2$ is a Gaussian. Equation (1) assumes a symmetric isobaric yield distribution about the most probable charge Z_p.

Using an iterative procedure with a nonlinear least-squares code [26], the values in Table II for parameters α_1–α_{10} were obtained by fitting the measured cross sections. In the first iteration cumulative as well as independent cross sections were used. The estimated cross sections for the isobaric progenitors were then subtracted from the cumulative yields. These now independent yields were then refitted. This procedure converged after three iterations.

In Fig. 2 we compare the isobaric yield data with the above parametrization. The data are presented as fractional isobaric yields, scaled to a common mass ($A = 51$) by the equation

$$F_{\rm cor}(Z_p - Z, A) = F_{\rm expt}((Z_p - Z),\ A)\frac{F_{\rm calc}((Z_p - Z), A = 51)}{F_{\rm calc}((Z_p - Z),\ A)}, \quad (3)$$

where $F_{\rm expt}$ and $F_{\rm calc}$ are the experimental and calculated cross sections divided by the calculated value $\sigma(A)$, respectively. Comparison with the previously reported distributions for 15–45 MeV/nucleon ^{12}C shows that the isobaric yield distributions are approximately independent of energy. The parameters characterizing the distribution such as the full width at half maximum (FWHM) and Z_p are constant within the limits of error. The only significant change is that as the energy increases to 90 MeV/nucleon the wings broaden, as signified by a decrease in the parameter α_8. Figure 3 shows the energy dependence of these parameters.

B. Mass yield distribution

By combining the cross sections of the unmeasured nuclides with the experimental cross sections, we can obtain an estimate of the total cross section at each product mass number A. A 20% uncertainty is assumed for those cross sections calculated using Eq. (1) on the basis of the agreement of the experimental yields with the isobaric yield distribution. The results are displayed in Fig. 4, where the curves represent cross sections obtained using Eq. (1) exclusively. It is seen the parametrization provides a good fit to the data.

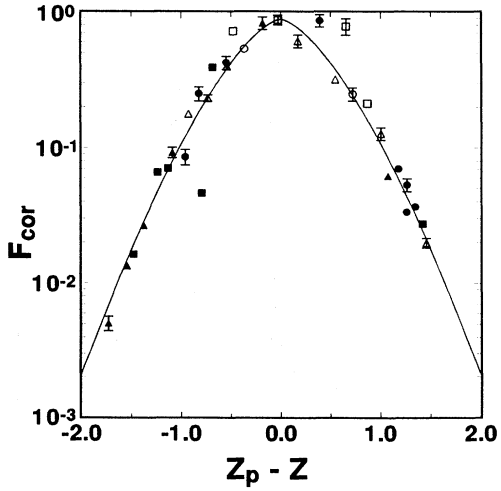

FIG. 2. Fractional isobaric yield distribution for the interaction of copper with 90 MeV/nucleon ^{12}C ions. The curve represents the fitted values from Eqs. (1) and (2) at $A = 51$; the data are scaled to $A = 51$. The different symbols indicate the product mass region: (•) $A = 22$–46, (▲) $A = 47$–57, and (■) $A = 58$–65. Open symbols represent independent yields.

Figure 4 shows the evolution of the mass yield distribution with increasing projectile energy, by comparison with similar results obtained at lower energies [19]. It is interesting to note that the basic shape of the distribution remains the same over the broad energy range covered in these studies. For each energy there is a peak several mass units lower than the target, then a smooth decrease to $A \approx 25$–30, and finally an upturn toward lower-mass products. This upturn is attributed to sequential fragment emission [27–29], which has been reported at these energies.

In spite of these overall similarities, the mass yield distribution does evolve with energy. It has been previously reported [19] that the peak in the distribution moves toward lower masses with increasing energy. This is shown more clearly in Fig. 5, where the evolution of the mean mass loss from the target with bombarding energy is displayed. The mass loss rises steeply between 15 and 45 MeV/nucleon and then only slightly between 45 and 90 MeV/nucleon. From Fig. 4 it is apparent that the minimum in the mass yield distribution moves toward lower masses with increasing energy. Also, the distribution becomes flatter with increasing energy. The slope in the exponential region of the distribution is a quantitative measure of this effect and has been proposed by Cumming *et al.* [30] as a measure of the excitation energy deposited in the composite system. These workers examined the slopes of this exponential region for reactions of copper with a variety of projectiles. Figure 6 presents a comparison of the present data with that summarized by Cumming *et al.* [30]. The data agree well with the Cumming systematics.

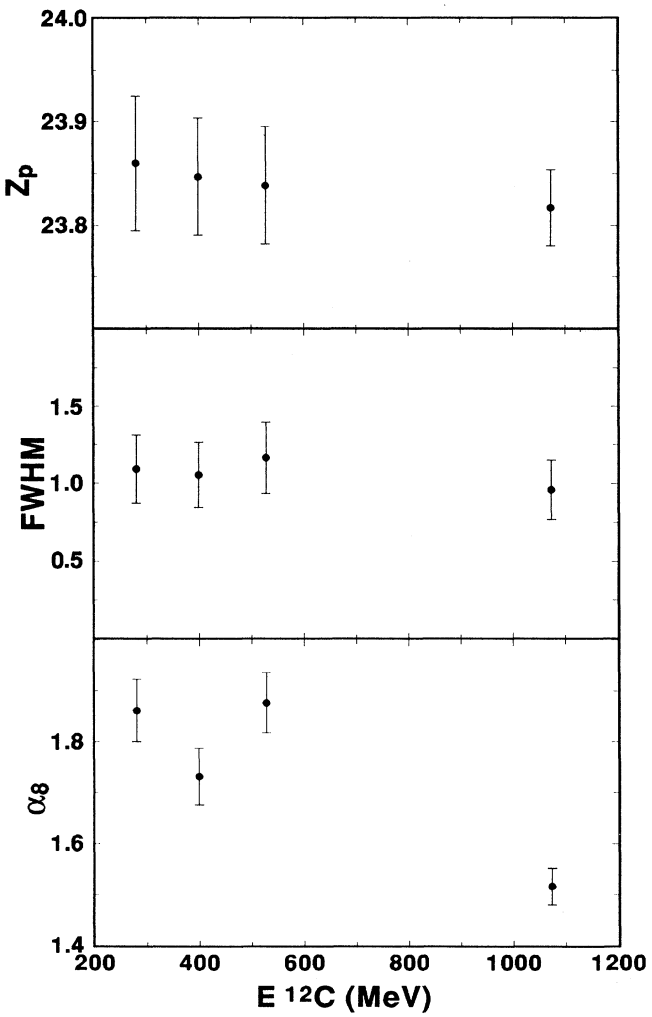

FIG. 3. Energy dependence of (a) Z_p, (b) the full width at half maximum, and (c) the parameter α_8, evaluated at $A = 51$.

C. Analysis of recoil-range data

Recoil-range studies have long been analyzed utilizing a two-step model approximation [31], where in the first,

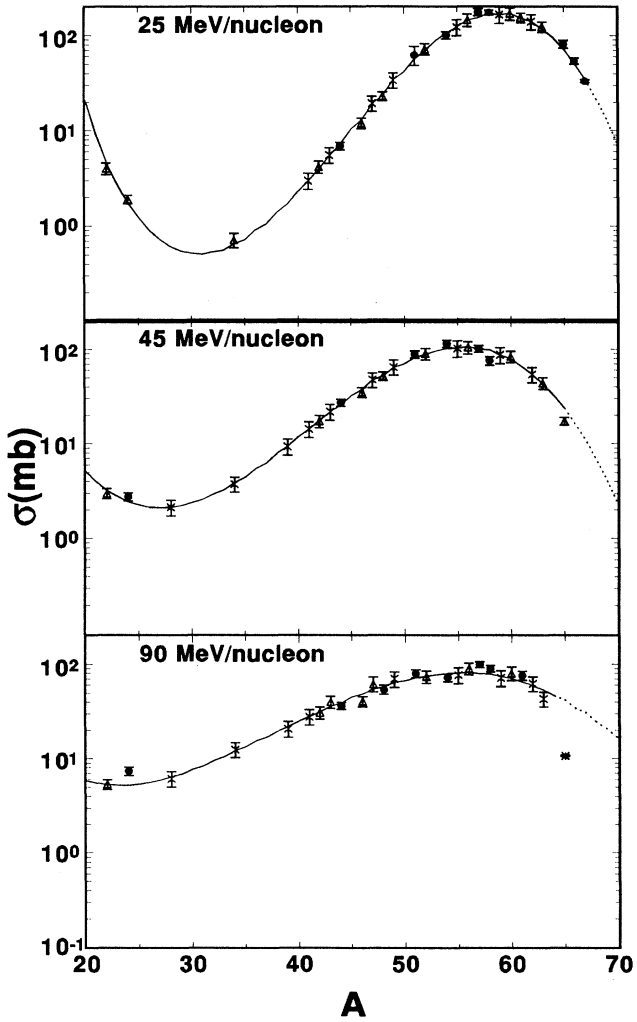

FIG. 4. Mass yield distributions for the interaction of copper with 25, 45, and 90 MeV/nucleon ^{12}C ions. The curves represent the calculated cross sections obtained from Eqs. (1) and (2). The points are the experimental cross sections corrected for unmeasured yields. The different symbols indicate the fraction that was measured: •, >50%; △, 20–50%; and *, <20%. The lower-energy data are from Ref. [19].

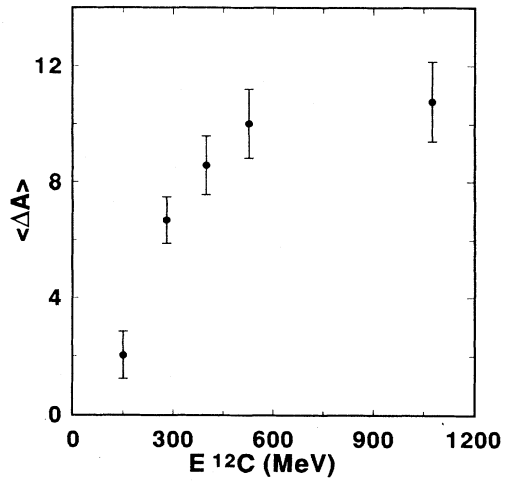

FIG. 5. Energy dependence of the mean mass loss from the target (ΔA).

fast step, the heavy residue acquires a velocity v, whose component along the beam direction is $v_{\|}$, and then deexcites by particle evaporation in the second, slower step, yielding a second velocity V, which is isotropic in the moving system or at least symmetric about 90°. It is possible to determine $v_{\|}$ and V from the recoil data using equations in which truncations of the variable η $(= v_{\|}/V)$ are assumed. Yet, for large F/B, these truncations prove incorrect since $\eta > 1$.

When the reactions involve large LMT, signified by large F/B, Winsberg and Alexander [32] have shown that V may be neglected. In this case the velocity corresponding to $v_{\|}$ is just FW. Recently, Whitfield and Porile [33] have tested this hypothesis employing Monte Carlo techniques. It was found that this assumption was valid, within statistical uncertainties, for the 45 MeV/nucleon ^{12}C + Cu reaction. On the other hand, the results for

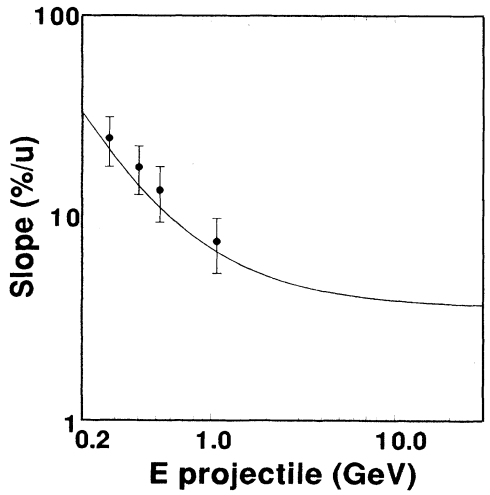

FIG. 6. Comparison of the slope from the exponential region of the mass yield distributions for 25–90 MeV/nucleon ^{12}C plus copper with Cumming [30] systematics.

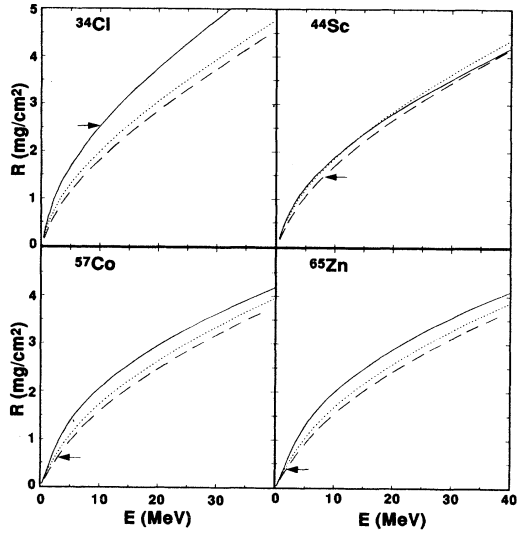

FIG. 7. Comparison of the range-energy relationship calculated from ZBL [37] transport equations (——) and those calculated using Northcliffe-Schilling [35] tables directly (· · · ·) and converting the path lengths to projected ranges using LSS [38] formalism (- - - - -). The arrows indicate the experimental FW values.

the 90 MeV/nucleon experiment indicated that $v_{\|}$ was overestimated by 5–6 % for $17 \leq Z_{\text{prod}} \leq 25$, but the correction decreased monotonically to $Z = 30$, where no correction is needed. The present data for 90 MeV/nucleon ^{12}C have been adjusted using these calculated factors. For those products far removed from the target, we obtained $v_{\|}$ by means of the Winsberg [34] analysis, which involves both $v_{\|}$ and V, because of the smaller F/B values for these product nuclides.

In past investigations range-energy conversions were performed using the Northcliffe-Schilling tables [35]. In recent years much work has been done in the area of range-energy relationships. These results have been summarized by Biersack and Ziegler [36]. It was found that the results from the Northcliffe-Schilling tables are inaccurate where the recoiling ion is not heavy compared with the target atom, $(M_1/M_2 < 3)$, where M_1 and M_2 are the masses of the ion and target, respectively. Since this ratio is <1 for nearly all experimental recoil products, we have used a more refined approach utilizing transport equations developed by Ziegler, Biersack, and Littmark (ZBL) [37]. We have generated range-energy tables by means of the code TRIM [37]. A comparison between the Northcliffe-Schilling range-energy curves [with and without path lengths corrected to projected ranges using the Lindhard-Scharff-Schiott (LSS) [38] formalism] and ZBL curves is shown in Fig. 7 for several products. The data from the interaction of copper with 15–45 MeV/nucleon ^{12}C ions have been reanalyzed with the ZBL equations. The effect of using the ZBL conversions compared with the Northcliffe-Schilling conversions is to reduce the resultant $v_{\|}$ by ~5% for the lighter reaction products (e.g., ^{42}K, ^{46}Sc), by up to ~12% for intermediate mass prod-

ucts (e.g., ^{51}Cr, ^{52}Mn), and by up to ~20% for the heaviest products (e.g., ^{61}Cu, ^{65}Zn).

In a thick-target, thick-catcher experiment, the $v_{\|}$ derived from the range data can also be affected if there is a signficant change in production cross section along the target depth [39]. By constructing excitation functions for each product nuclide using the results from the 15–90 MeV/nucleon data, we can estimate the variation in cross section between the upstream and downstream faces of the target. In order to correct for this effect we have utilized a formula given by Hazan and Blann [40],

$$R = FW[(su + sd)/2sd], \quad (4)$$

where su and sd are the cross sections at the upstream and downstream faces of the target, respectively. This equation is an approximation, which is valid for our data, to a more complete formula that applies when the difference between su and sd is much larger than the smaller of these two cross sections. We have applied this correction to those data for which the difference between su and sd exceeds 50% of the uncertainty associated with the experimental cross section.

None of the present data or our earlier data for 35 or 45 MeV/nucleon required correction for this effect. For the 15 MeV/nucleon data the largest corrections were made for those products 5–10 mass units removed from the target as well as for ^{65}Zn. These corrections varied between 10% and 20%. For the remainder of the products the correction was less than 4% in all cases. At 25 MeV/nucleon ^{65}Zn again required a large correction of ~20%, while no other product required a correction larger than 5%.

The resulting $v_{\|}/v_{\rm CN}$ values are shown for several energies in Fig. 8 as a function of the mass loss from the target, where $v_{\rm CN}$ is the velocity of the presumed compound nucleus. It is apparent that with increasing bombarding energy we see decreasing amounts of fractional velocity transfer. However, each of the distributions shows very similar characteristics. The remnant velocity increases with increasing mass loss to a plateau region for those products farthest removed from the target. We believe these effects to have a geometrical origin, where the near-target products are produced primarily in very peripheral interactions where very little velocity or momentum is transferred from the projectile to the target, while those in the plateau region are produced in more central collisions, as proposed by Pieńkowski *et al.* [11].

The model most commonly used in the interpretation of $v_{\|}$ is one in which the initial interaction is viewed as involving incomplete fusion with beam velocity particles of total mass Δm escaping at 0° [7]. Δm can be estimated using the relationship

$$\frac{v_{\|}}{v_{\rm CN}} = \frac{(A_p - \Delta m)}{A_p}, \quad (5)$$

where A_p is the projectile mass. With knowledge of Δm we can in turn determine the mass of the composite system $A_{\rm comp}$. The variation in $\langle A_{\rm comp}\rangle$ with bombarding energy is depicted in Fig. 9. At the lowest energy we see

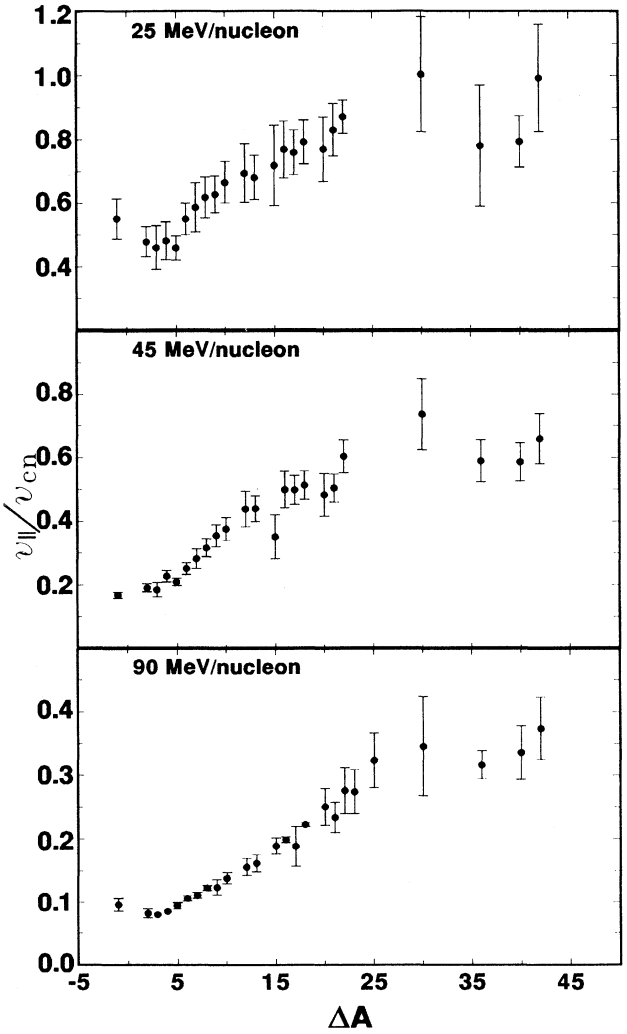

FIG. 8. Fractional velocity transfer for the interaction of Cu with 25, 45, and 90 MeV/nucleon ^{12}C ions, where ΔA is the mass loss from the target.

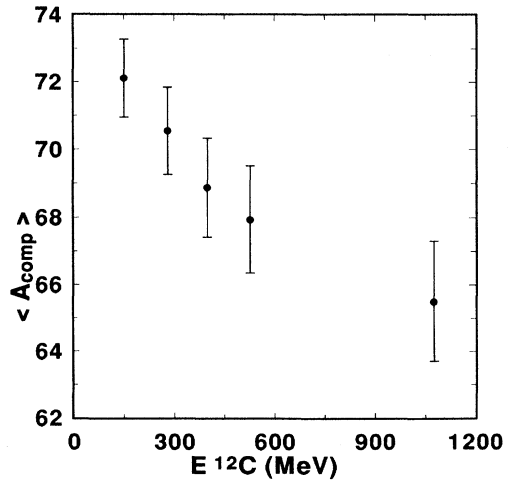

FIG. 9. Energy dependence of $\langle A_{\rm comp}\rangle$, the mean mass of the composite system remaining after the initial interaction.

that on average ~8 projectile nucleons are captured by the target. This number decreases nearly linearly with increasing projectile energy, and at the highest energy only ~2 projectile nucleons are captured. This decrease demonstrates the increasingly incomplete fusion that occurs as the projectile energy increases. The product of these two values, $v_{\|}$ and A_{comp}, is the linear momentum transferred from the projectile to this composite system.

The results depend on the validity of Eq. (5). Consider first the assumption that particles emitted in the initial interaction have beam velocities. It has been shown [41] that if the mass of the emitted particle is similar to the mass of the projectile, this assumption is valid. Yet, as the mass of the emitted particles decreases, the velocity decreases, where those projectile residues with significant mass loss have a velocity of approximately 90% beam velocity. Therefore, from momentum balance, we expect slightly greater momentum transfer to the composite system for those interactions where beamlike particles are emitted with lower than beam velocity. For example, for $\Delta m = 4$ and 90% beam velocity, the error in LMT is ~3%.

The second point to address is the emission angle of these projectilelike fragments. It has been reported [42] that the velocity spectrum of evaporation residues should be a Gaussian centered on $v_{\|} = v_R \cos\theta$, where v_R is the velocity of the composite system and θ is the detection angle in the laboratory. Using $\rho = v_R/v_{\text{CN}}$ and

$$\frac{P_{\|}}{P_{\text{CN}}} = \rho \frac{A_T}{A_T + (1-\rho)A_p}, \tag{6}$$

where A_T is the mass of the target, and simple kinematic relationships we can calculate the difference in the momentum transfer for projectile remnants emitted at θ and at 0°. This difference is also mass dependent; therefore, we have also looked at a variety of ejectile masses Δm.

For small Δm ($\approx$2) the difference is less than 1% for emission angles between 10° and 45°. At intermediate ejectile masses ($\Delta m \approx$6) this difference increases to 2–15% for the same angular range, while for large Δm ($\approx$10) the differences for angles between 2.5° and 20° is 2–68%. Therefore the calculated momentum using the present assumptions would be significantly underestimated for interactions where large ejectile masses are emitted at large angles.

The angular distributions for complex ejectiles (with energy spectra centered at beam velocities) have been shown to peak near the classical grazing angle [43]. The grazing angle for the ^{12}C + Cu reaction at 15–90 MeV/nucleon varies between 11° and 2°. Assuming these angles to correspond to the peaks in the angular distributions and assuming an average mass of the ejectile, $\langle \Delta m \rangle$, at each energy, we can estimate the error associated with the assumption that the ejectiles are emitted at 0°. We find that the error varies between 1% and 2% for the energy range of present interest. Therefore, combining the results for ejectiles emitted with lower than beam velocity and at angles other than 0°, it seems reasonable to analyze the data utilizing the aforementioned assumptions.

D. Linear momentum transfer

By weighting the individual values of $P_{\|}$ by their experimental cross sections we can obtain the mean LMT at each bombarding energy. The results are displayed in Fig. 10. The average LMT values increase from 15 to 25 MeV/nucleon to a maximum of approximately 1.4 GeV/c. The $\langle$LMT$\rangle$ then decreases nearly linearly with increasing projectile energy. Batsch *et al.* [12] and Pieńkowski *et al.* [11] have examined both projectile mass dependence as well as energy dependence of the average LMT using Cu targets. Comparison between the various data for $\langle$LMT$\rangle$ is presented in Fig. 11. For each of the different projectiles there appears to be a maximum at ~20–25 MeV/nucleon. There also appears to be a projectile dependence on the amount of momentum which can be transferred. The results presented in Fig. 11 seem to demonstrate that as the mass of the projectile increases there is increasing incomplete fusion. The effect

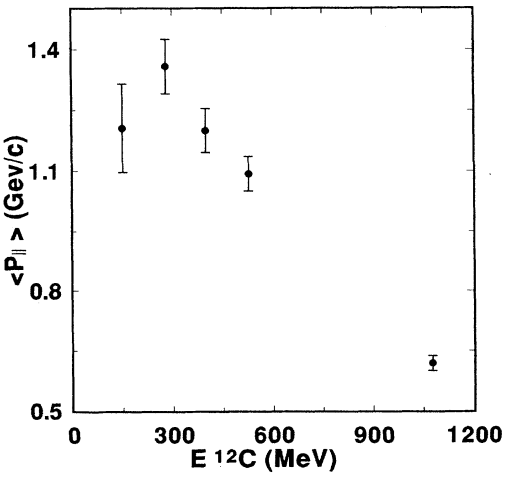

FIG. 10. Energy dependence of the mean linear momentum transfer $\langle$LMT$\rangle$.

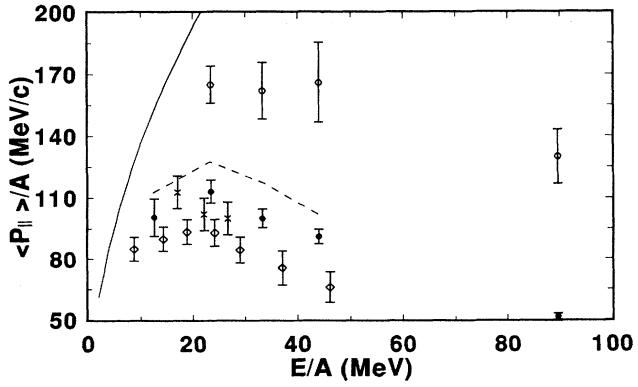

FIG. 11. Variation with projectile energy of the linear momentum transfer per incident projectile nucleon. The solid line represents full momentum transfer. The different symbols represent the various projectile-Cu combinations: (•) average ^{12}C, (○) maximum ^{12}C, (∗) ^{14}N [11], and (◇) ^{20}Ne [11]. The dashed line depicts the ^{12}C + Ag data [17].

of analyzing the ^{14}N and ^{20}Ne data using ZBL range-energy conversions rather than Northcliffe-Schilling conversions, which is the method used for these data, would be to reduce the $\langle P_{\|}/A \rangle$ values. Therefore the use of the more accurate range-energy relation would enhance the observed trend. The dashed line in Fig. 11 shows the results from the interaction of ^{12}C and Ag at 15–45 MeV/nucleon [17]. These data have been reduced by 15% to account in an approximate way for the use of these different range-energy relations. It appears that there also is a target mass dependence to the amount of linear momentum transferred per incident nucleon. LaRana *et al.* [44] have proposed that this behavior arises from the increased volume of the larger target nucleus so that the projectile spends more time under the influence of the target's mean field and in turn deposits more momentum.

If we define the plateau region in the fractional velocity transfer distribution as representing those products produced in central collisions, we can find the maximum momentum transfer for each of the bombarding energies. Since there is no definable plateau at 15 MeV/nucleon, these data will be excluded from the discussion of maximum LMT. The $\langle P_{\|}^{\max} \rangle$ for the 25–90 MeV/nucleon reactions are displayed in Fig. 11. It may be noted that even though the average LMT decreases with increasing projectile energy, the $\langle P_{\|}^{\max} \rangle$ values for the 25–45 MeV/nucleon data remain constant at approximately 170 MeV/c per incident nucleon and then decrease to ~130 MeV/c per incident nucleon for the 90 MeV/nucleon data. This result appears to point to the increasing importance of peripheral interactions in producing the detected products at higher projectile energies. Similar results have also been found for much heavier targets [43, 45]. It is interesting to note that although $\langle P_{\|} \rangle / P_{\rm CN}$ are low relative to the Leray systematics [7], there is good agreement in the comparison with $\langle P_{\|}^{\max} \rangle / P_{\rm CN}$, as is shown in Fig. 12.

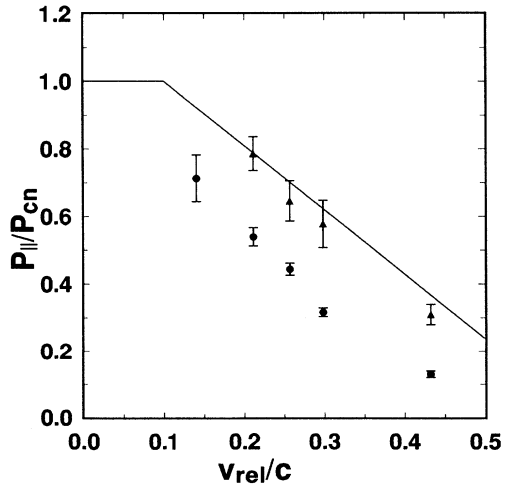

FIG. 12. Comparison of the average (•) and maximum (▲) LMT for ^{12}C + Cu interactions with Leray systematics (——).

E. Comparison with cascade-evaporation calculations

As the beam energy increases to 90 MeV/nucleon, the reaction evolves from mean-field to nucleon-nucleon dynamics. Therefore intranuclear cascade-evaporation calculations should provide a reasonable prediction of the mass yield distribution and the recoil data at the highest energy. We have utilized the cascade code ISABEL [46] to generate the LMT and E^* distributions and, when coupled with the evaporation code EVA [47], the mass yield distribution. Comparisons were made using 10 000 cascade-evaporation events. Figure 13 compares the experimental and calculated mass yield distributions at 45 and 90 MeV/nucleon.

At 90 MeV/nucleon the calculation predicts the general shape of the distribution quite well. Although the cross sections of near-target products are somewhat overpredicted and those of low-mass products underpredicted, the exponential spallation region is well represented by the cascade-evaporation model. The underestimation for those products far removed from the target, as was previously mentioned, is a consequence of binary fragmentation of the composite system, which is not incorporated into these codes. It appears that between 90 and 45 MeV/nucleon the model breaks down [Fig. 13(b)]. This suggests that at 45 MeV/nucleon mean-field effects indeed still play a prominent role in the reaction mechanism.

Figure 14 displays a comparison between experimental and calculated values for the fractional velocity transfer.

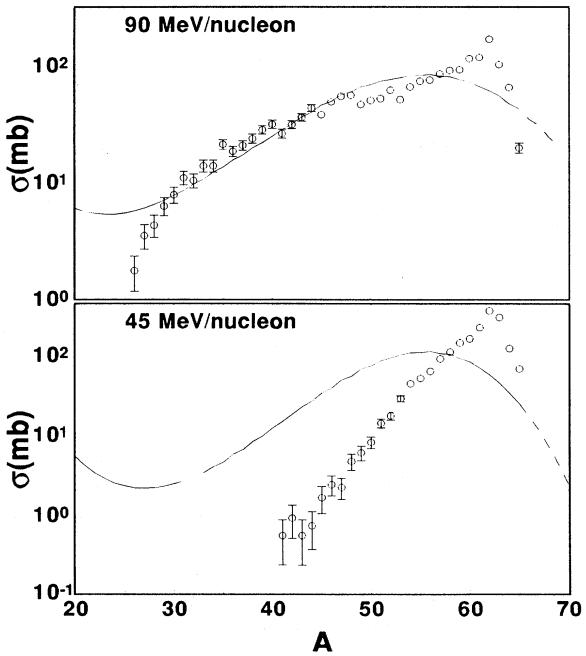

FIG. 13. Comparison of the experimental and ISABEL-EVA (○) calculated mass yield distribution for (a) 90 MeV/nucleon ^{12}C + Cu and (b) 45 MeV/nucleon ^{12}C + Cu. The uncertainties in the calculated cross sections reflect the number of events leading to a particular product.

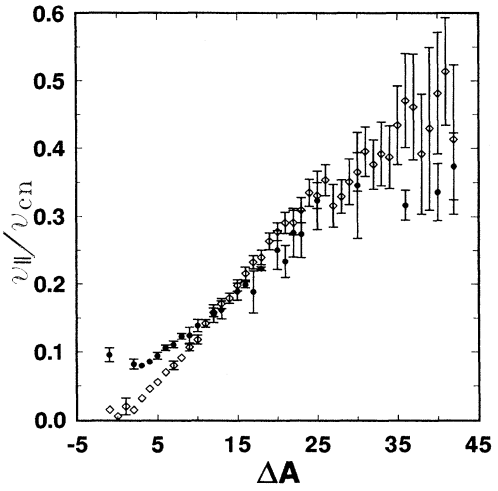

FIG. 14. Comparison of the experimental (•) and calculated (◇) fractional velocity transfer for 90 MeV/nucleon ^{12}C.

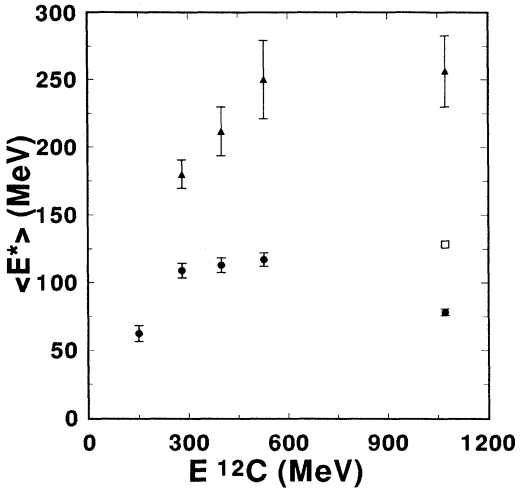

FIG. 15. Dependence of the mean (•) and maximum (▲) excitation energy of the composite system on the ^{12}C bombarding energy. The open square is the ISABEL-EVA value.

The calculation seems to predict the experimental data for $\Delta A = 10$–30 fairly well, yet for those products farther removed from the target the fractional velocity transfer is overestimated somewhat. In turn, near-target product velocity transfers are severely underestimated. The appearance of a possible plateau in the distribution is also not predicted by the calculation, although the statistical uncertainties for these low-yield products are large.

F. Excitation energy deposition

Various methods have been used to extract the excitation energy deposited in the composite system from the type of data presented in this work. Most of these methods are based on variants of the proportionality between fractional momentum transfer and fractional excitation energy transfer [48]. In our previous work at lower energies we used a relation based on Leray's incomplete fusion model [7]:

$$E^* = \left(\frac{P_\parallel}{P_{\rm CN}}\right)\left(\frac{A_T}{A'_p + A_T}\right) E_{\rm lab} + Q,$$
$$Q = \Delta m(-7\ {\rm MeV}), \tag{7}$$

where $A'_p = A_p - \Delta m$ and $E_{\rm lab}$ is the total projectile kinetic energy in the laboratory system. The Q value is calculated assuming the projectile nucleons not captured by the target escape as free nucleons. This relation can also be applied to the present data.

Figure 15 shows the variation with bombarding energy of the mean excitation energy $\langle E^* \rangle$. There appears to be an increase to approximately 120 MeV at 45 MeV/nucleon and then a decrease between this energy and 90 MeV/nucleon. This decrease appears to be unphysical and is inconsistent with the results in Fig. 6, which suggest a continuing increase in $\langle E^* \rangle$ with bombarding energy in this regime. Figure 15 also displays the mean excitation energy for central collisions, $\langle E^*_{\rm cen} \rangle$, where a sharp increase to 250 MeV may be seen between 25 and 45 MeV/nucleon. While $\langle E^*_{\rm cen} \rangle$ does not decrease above this energy, it does not exhibit a significant further increase.

In order to understand the observed trend it is necessary to examine the E^* values obtained at 90 MeV/nucleon in further detail. This is done in Fig. 16, which shows the E^* for the formation of individual products versus mass loss from the composite system. The excitation energy increases with the mass loss over most of the mass region and, as indicated in the figure, is consistent with a value of 6.8 MeV/emitted nucleon. This value is too low to permit the formation of the various products by sequential evaporation of single nucleons, which one expects to be the dominant mechanism at this energy.

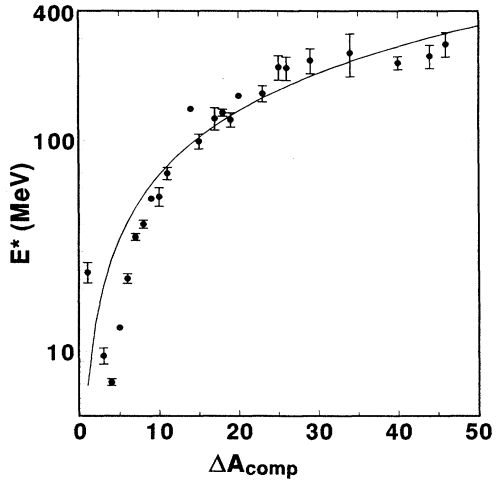

FIG. 16. Variation of the mean excitation energy with mass loss from the composite system for the interaction of copper with 90 MeV/nucleon ^{12}C ions. The solid curve corresponds to E^*/emitted nucleon = 6.8 MeV.

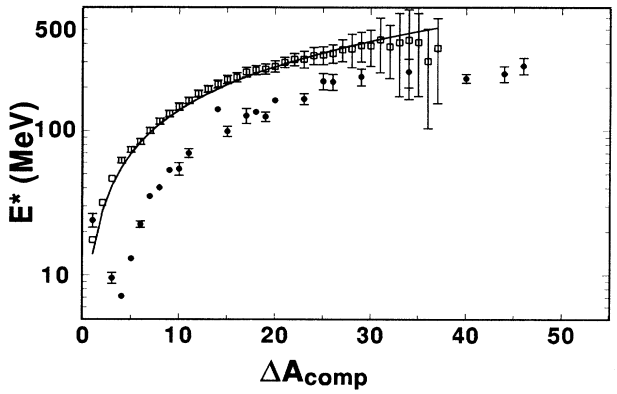

FIG. 17. Comparison of the variation of the excitation energy with mass loss from the composite system for the experimental results (•) and ISABEL-EVA calculation (□) at 90 MeV/nucleon. The solid curve through the calculated values is a fit corresponding to 14 MeV/emitted nucleon.

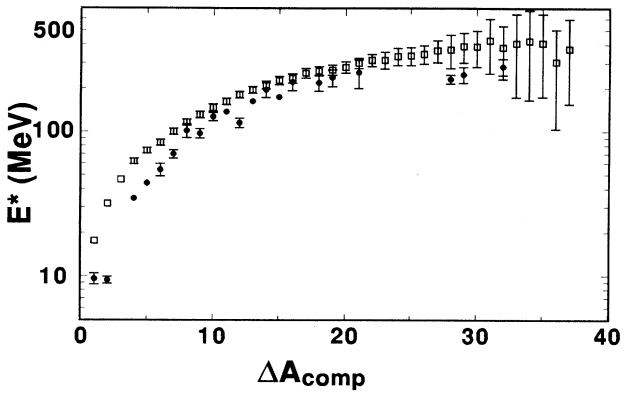

FIG. 19. Data from Fig. 17, where the experimental E^* values have been replotted versus mass loss from the composite nuclei given by ISABEL-EVA.

Thus the downturn in $\langle E^* \rangle$ displayed in Fig. 15 can be attributed to uniformly low E^* values for all products.

Further insight into the source of this problem can be obtained by comparison of the E^* values with those predicted by the ISABEL code, as shown in Fig. 17. The calculated values were obtained by averaging the excitation energies for each ISABEL remnant, which according to EVA, deexcited to form the products in question. The calculated E^* are substantially larger than the experimental values, although they display a similar mass dependence. The solid curve through the calculated points corresponds to an energy of 14 MeV/emitted nucleon. The average excitation energy is 128±2 MeV; as shown in Fig. 15, this value represents a reasonable continuation of the trend displayed by the lower-energy data.

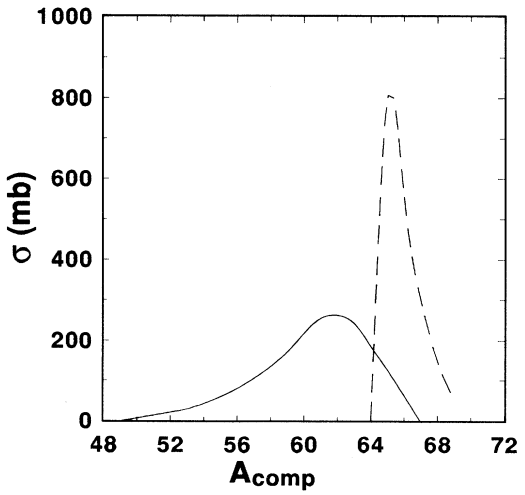

FIG. 18. Mass distributions of the experimental (- - - - -) and calculated (——) composite system for 90 MeV/nucleon ^{12}C + Cu.

We believe that the above discrepancy reflects a breakdown in the assumption used to derive the excitation energy from the data. Equations (5) and (7) imply that the only mechanism of energy transfer to the composite system involves the capture of projectile nucleons. However, additional mechanisms become important at energies where nucleon-nucleon collisions become important. These include the energy transferred to target nucleons by collisions with projectile nucleons as well as the energy of the holes in the Fermi sea left by knocked out target nucleons. The importance of these processes can be seen in a comparison of the calculated and experimental mass distributions of the composite system, shown in Fig. 18. While the experimental distribution necessarily requires the composite nuclei to be more massive than the target, this turns out not to be so for the ISABEL distribution, indicating that nucleon knockout is an important mechanism for energy deposition. The overestimation of the masses of the composite nuclei accounts for most of the discrepancy between the calculated and experimental E^*. This can be seen in Fig. 19, where the results in Fig. 17 are replotted versus mass loss from the composite nuclei obtained from ISABEL, for both sets of E^* values. The calculated E^* are now only slightly larger than the experimental values.

V. CONCLUSIONS

The interaction of copper with 90 MeV/nucleon ^{12}C ions has been studied and compared with similar data obtained by our group at lower energies. The isobaric yield distribution remains essentially unchanged in this energy regime. The mass yield distribution, on the other hand, displays considerable variation: With increasing projectile energy, the minimum and maximum of the distribution move toward lower masses, while the distribution flattens out. This leads to a decrease in the slope in the exponential region of the distribution with increasing bombarding energy.

The $\langle$LMT$\rangle$ increases to a maximum of approximately 1.4 GeV/c at 25 MeV/nucleon and then decreases mono-

tonically to 90 MeV/nucleon. For central collisions there seems to be a limit to the LMT of ~170 MeV/c per incident nucleon. Comparisons for these central collisions are in good agreement with Leray systematics. There also appears to be a dependence of the ⟨LMT⟩ on projectile as well as target identity.

Comparisons have been made between experimental results and intranuclear cascade-evaporation calculations for the 90 MeV/nucleon interaction. The calculation reproduces the mass yield distribution well for those products in the exponential spallation region. The fractional velocity transfer distributions are approximately represented by the calculation. The calculated excitation energies are larger than the experimental values, reflecting the importance of energy transfer processes not included in the extraction of E^* values from the data.

ACKNOWLEDGMENTS

We wish to thank R. Ronningen and all the members of the NSCL who contributed their assistance and cooperation to this project. This work was supported by the U.S. Department of Energy.

[1] J. Galin *et al.*, Phys. Rev. Lett. **48**, 1787 (1982).
[2] G. Nebbia *et al.*, Z. Phys. A **311**, 247 (1983).
[3] J. L. Laville *et al.*, Phys. Lett. **138B**, 35 (1984).
[4] J. Jastrebski, P. P. Singh, T. Moróz, H. J. Karwowski, S. E. Vigdor, and M. Fatyga, Phys. Lett. **136B**, 153 (1984).
[5] V. E. Viola, Nucl. Phys. **A471**, 53c (1987).
[6] M. B. Tsang *et al.*, Phys. Lett. **134B**, 169 (1984).
[7] S. Leray, J. Phys. C **4**, 275 (1986).
[8] F. Saint-Laurent *et al.*, Phys. Lett. B **202**, 190 (1988).
[9] D. X. Jiang *et al.*, Nucl. Phys. **A503**, 560 (1989).
[10] D. H. E. Gross, Z. Xiao-ze, and X. Shu-yan, Phys. Rev. Lett. **56**, 1544 (1986).
[11] L. Pieńkowski, J. Jastrebski, W. Kurcewicz, A. Gizon, J. Blachot, and J. Crancon, Phys. Rev. C **43**, 1331 (1991).
[12] T. Batsch *et al.*, Phys. Lett. B **189**, 287 (1987).
[13] T. Lund, D. Molzahn, R. Brandt, B. Bergersen, D. Eriksen, E. Hagebø, I. R. Haldorsen, T. Bjørnstad, and C. Richard-Serre, Phys. Lett. **102B**, 239 (1981).
[14] T. Lund, D. Molzahn, B. Bergersen, E. Hagebø, I. R. Haldorsen, and C. Richard-Serre, Z. Phys. A **306**, 43 (1982).
[15] A. Lleres, J. Blachot, J. Crancon, A. Gizon, and H. Nifenecker, Z. Phys. A **312**, 177 (1983).
[16] L. Kowalski, P. E. Haustein, and J. B. Cumming, Phys. Rev. Lett. **51**, 642 (1983).
[17] Y. H. Chung, S. Y. Cho, and N. T. Porile, Nucl. Phys. **A533**, 170 (1991).
[18] S. Y. Cho, Y. H. Chung, N. T. Porile, and D. J. Morrissey, Phys. Rev. C **36**, 2349 (1987).
[19] S. Y. Cho, N. T. Porile, and D. J. Morrissey, Phys. Rev. C **39**, 2227 (1989).
[20] F. Hubert, A. Fleury, R. Bimbot, and D. Gardes, Ann. Phys. (Paris) **5**, 1 (1980).
[21] T. Routti and S. G. Prussin, Nucl. Instrum. Methods **72**, 125 (1969).
[22] J. B. Cumming, National Academy of Sciences Report No. NAS-NS-3107, 1962 (unpublished), p. 25.
[23] U. Reus and W. Westmeier, At. Data Nucl. Data Tables **29**, 2 (1983).
[24] G. Rudstam, Z. Naturforsch. **219**, 1027 (1966).
[25] N. T. Porile, G. D. Cole, and C. R. Rudy, Phys. Rev. C **19**, 2288 (1979).
[26] J. B. Cumming, P. E. Haustein, R. W. Stoenner, L. Mausner, and R. A. Naumann, Phys. Rev. C **10**, 739 (1974).
[27] R. Trockel *et al.*, Phys. Rev. Lett. **59**, 2844 (1987).
[28] K. Grotwoski *et al.*, Phys. Lett. B **223**, 287 (1989).
[29] R. Bougault, J. Colin, F. Delaunay, A. Genoux-Lubain, A. Hajfani, C. Le Brun, J. F. Lecolley, M. Louvel, and J. C. Steckmeyer, Phys. Lett. B **232**, 291 (1989).
[30] J. B. Cumming, P. E. Haustein, T. J. Ruth, and G. J. Virtes, Phys. Rev. C **17**, 1632 (1978).
[31] N. Sugarman, M. Campos, and K. Wielgoz, Phys. Rev. **101**, 388 (1956).
[32] L. Winsberg and J. M. Alexander, Phys. Rev. **121**, 518 (1961).
[33] J. P. Whitfield and N. T. Porile, Nucl. Phys. **A550**, 553 (1992).
[34] L. Winsberg, Nucl. Instrum. Methods **150**, 465 (1978).
[35] L. C. Northcliffe and R. F. Schilling, Nucl. Data Tables A **7**, 233 (1970).
[36] J. F. Ziegler and J. P. Biersack, in *The Stopping and Range of Ions in Matter, Treatise on Heavy-Ion Science*, edited by D. A. Bromley (Plenum, New York, 1985), Vol. 6, p. 95.
[37] J. F. Ziegler, J. P. Biersack, and U. Littmark, in *The Stopping and Ranges of Ions in Matter* (Pergamon, New York, 1985), Vol. 1.
[38] J. Lindhard, M. Scharff, and H. E. Schiott, K. Dan. Vidensk. Selsk. Mat. Fys. Medd. **33**(14), 1 (1963).
[39] N. T. Porile, Phys. Rev. **127**, 244 (1962).
[40] J. Hazan and M. Blann, Phys. Rev. **137**, B1202 (1965).
[41] C. K. Gelbke, C. Olmer, M. Buenerd, D. L. Hendrie, J. Mahoney, M. C. Mermaz, and D. K. Scott, Phys. Rep. **42**, 311 (1978).
[42] H. Morgenstern, W. Bohne, K. Grabisch, D. G. Kovar, and H. Lehr, Phys. Lett. **113B**, 463 (1982).
[43] M. Fatyga, H. J. Karwowski, K. Kwiatkowski, L. Nowicki, and V. E. Viola, Phys. Rev. C **35**, 568 (1987).
[44] G. LaRana *et al.*, Nucl. Phys. **A407**, 233 (1983).
[45] M. Conjeaud *et al.*, Phys. Lett. **159B**, 244 (1985).
[46] Y. Yariv and Z. Fraenkel, Phys. Rev. C **20**, 2227 (1979); **24**, 488 (1981).
[47] I. Dostrovsky, Z. Fraenkel, and G. Friedlander, Phys. Rev. **116**, 683 (1959).
[48] N. T. Porile, Phys. Rev. **120**, 572 (1960).